

Supplementary Figures and Legends

Fig. S1

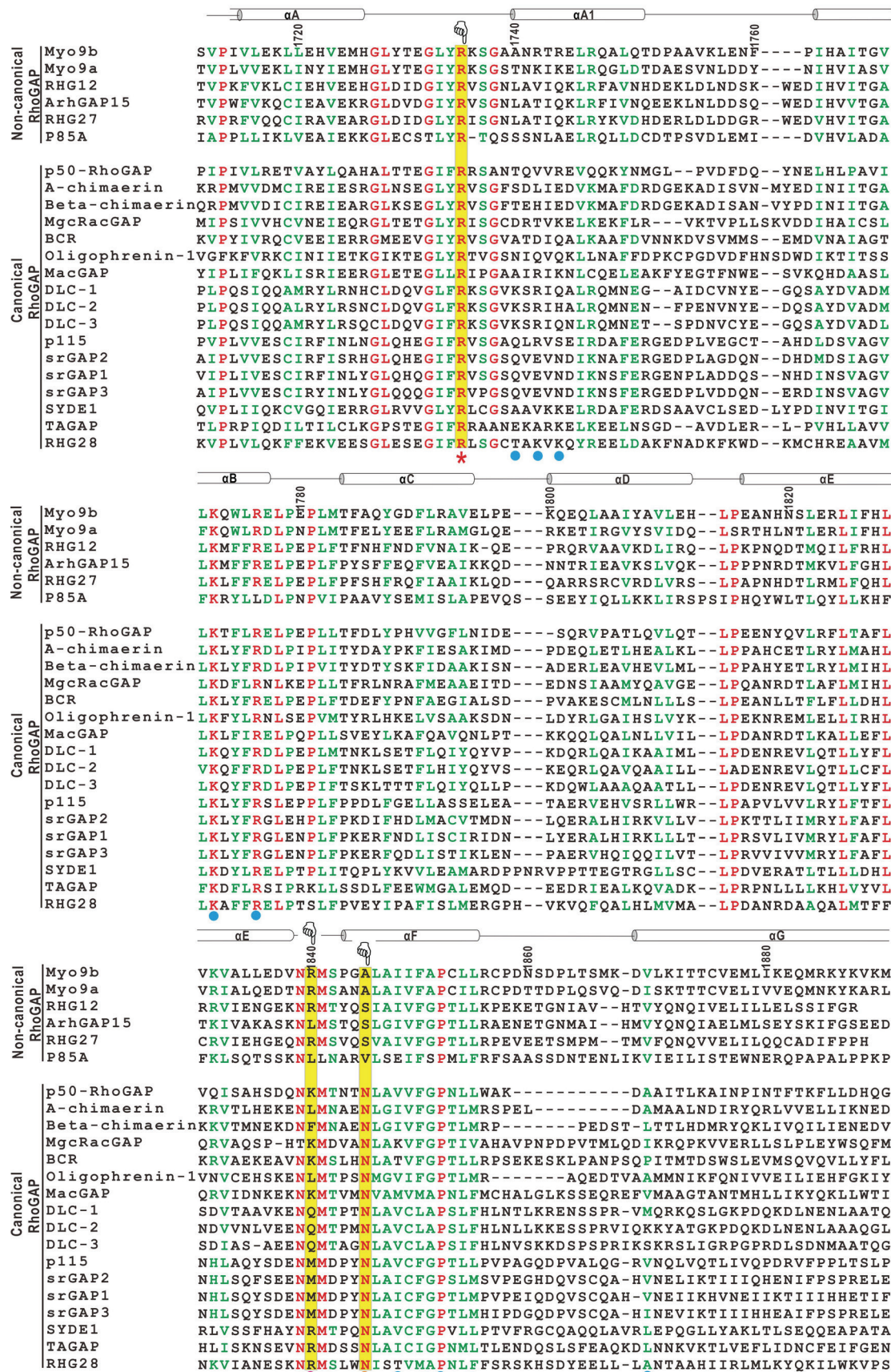


Fig. S1. Structure-based sequence alignment of the RhoGAP domains from different human proteins. The identical and highly conserved residues are colored in red and green, respectively. The residue numbers and the secondary structures of Myo9b-RhoGAP are marked on the top, and the residues involved in the three interaction sites for RhoA are highlighted with blue dots at the bottom. Consistent with our previous studies, the residues of Myo9b-RhoGAP in the interaction Site 1 (at the beginning of α A1) are not highly conserved, indicating that this is the key site to determine the specific activity of Myo9b-RhoGAP toward RhoA. The catalytic arginine-finger, the auxiliary arginine finger and the essential asparagine in the RhoGAP domains are highlighted with a red star, purple dot and yellow dot, respectively, at the bottom. Note that, a number of the RhoGAP domains do not contain the essential asparagine and some of them possess an additional arginine at the position corresponding to the second arginine finger found in Myo9b-RhoGAP, indicating that the dual-arginine-finger catalytic mechanism may be applicable to these RhoGAP domains. The NCBI accession numbers of these human proteins are: Myo9b (NM_004145.3), Myo9a (NM_006901.3), RHG12 (NM_018287.6), ArhGAP15 (NM_018460.3), RHG27 (NM_199282.2), p85A (NM_181523.2), p50-RhoGAP (NM_004308.3), A-chimaerin (NM_001822.5), Beta-chimaerin (NM_004067.3), MgcRacGAP (NM_013277.4), BCR (NM_004327.3), Oligophrenin-1 (NM_002547.2), MacGAP (NM_033515.2), DLC-1 (NM_006094.4), DLC-2 (NM_178006.3), DLC-3 (NM_014725.4), p115 (NM_001666.4), srGAP2 (NM_015326.4), srGAP1 (NM_020762.2), srGAP3 (NM_014850.3), SYDE1 (NM_033025.5), TAGAP (NM_054114.4), and RHG28 (XM_005258144.1).

Fig. S2

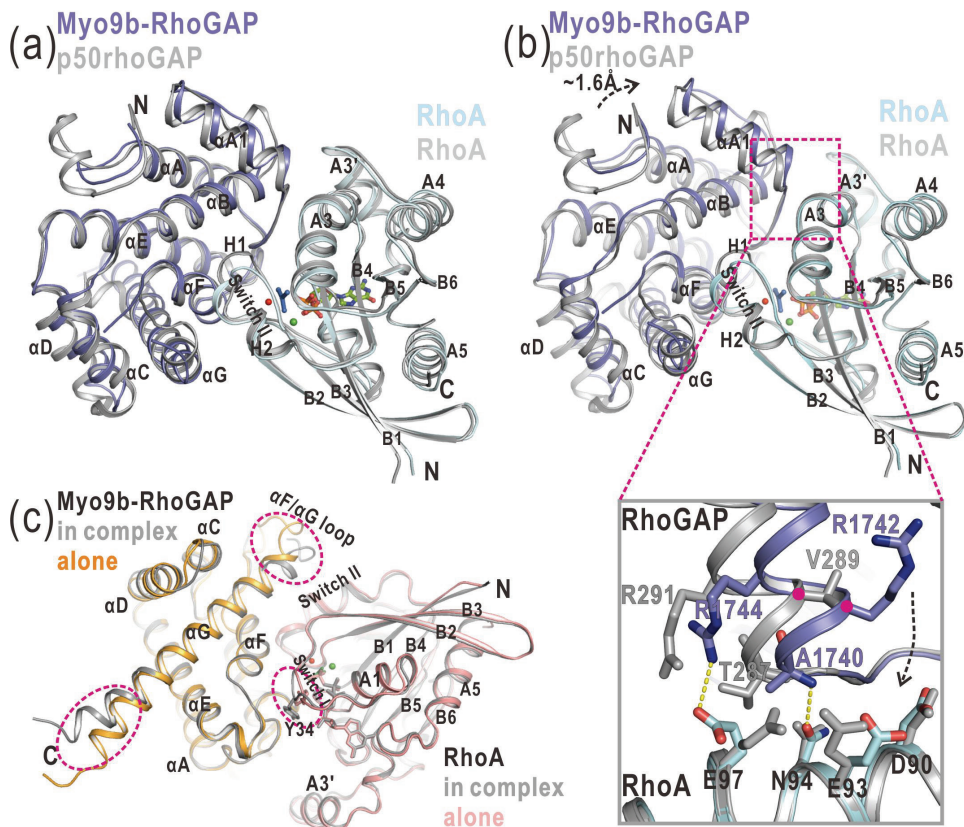


Fig. S2. Structural comparison of the Myo9b-RhoGAP/RhoA complex with the p50-RhoGAP/RhoA complex (a-b) and of Myo9b-RhoGAP and RhoA in the complex with their free forms (c). (a) A ribbon diagram of the structures of the Myo9b-RhoGAP/RhoA complex and the p50-RhoGAP/RhoA complex (PDB code: 1OW3) by the superimposition of both the RhoGAP domain and RhoA. The Myo9b-RhoGAP/RhoA complex is colored as shown in Fig. 1c and the p50-RhoGAP/RhoA complex is colored in gray. The secondary structures and the N- and C-termini of the domains are marked. (b) A ribbon diagram of the structures of the two complexes by the superimposition of RhoA alone. Note that, Myo9b-RhoGAP moves more closely to RhoA, which might be caused by the cluster of the specific electrostatic interactions between them at Site 1 (highlighted by a dash box). In a close-up view of the interaction Site 1 in the two complex structures, one of the positively charged residues (R1742) in Myo9b-RhoGAP is replaced by a valine (V289) in p50-RhoGAP (marked with pink dots), which would likely weaken the interaction Site 1 in the p50-RhoGAP/RhoA complex. (c) Structural comparison of Myo9b-RhoGAP and RhoA in the complex with their free forms (Myo9b-RhoGAP, PDB code: 5C5S; RhoA, PDB code: 1A2B), respectively. The Myo9b-RhoGAP/RhoA complex is colored in gray, Myo9b-RhoGAP alone is colored in orange, and RhoA bound with a GTP analogue is colored in pink. The regions exhibit local structural changes are highlighted by dash circles.

Fig. S3

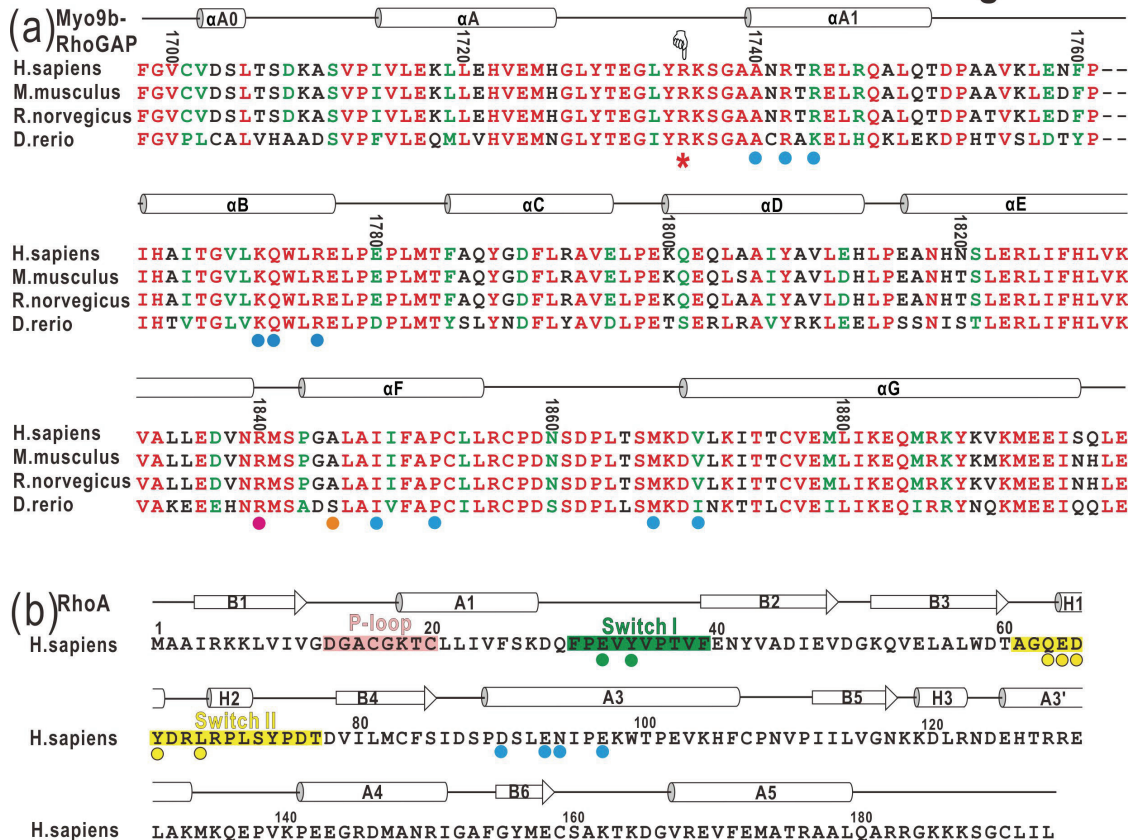


Fig. S3. Structure-based sequence alignment of Myo9b-RhoGAP from different species (a) and the sequence of RhoA used in this study (b). (a) In this sequence alignment, the identical and highly conserved residues are colored in red and green, respectively. The residue numbers and the secondary structures of Myo9b-RhoGAP are marked on the top, and the residues involved in the three interaction sites for RhoA are highlighted with blue dots at the bottom. The catalytic arginine-finger, the auxiliary arginine finger and the position for the essential asparagine in the RhoGAP domains are highlighted with a red star, purple dot and yellow dot, respectively. Note that, the hydrophobic residues for binding to RhoA are highly conserved and the two arginine fingers of Myo9b-RhoGAP are also conserved. *Homo sapiens* (H.sapien) (NM_004145.3), *Mus musculus* (M.musculus) (NM_001142323.1), *Rattus norvegicus* (R.norvegicus) (NM_001271066.1), and *Danio rerio* (D.rerio) (XM_005171334.2). (b) The residue numbers and the secondary structures of human RhoA (NM_001664.2) are marked on the top. The Switch I and II and P-loop of RhoA are highlighted with a green, yellow and pink box, respectively. The residues in Switch I and II and the A3 helix for the interaction interface packing are marked with green, yellow and blue dots, respectively, at the bottom.

Fig. S4

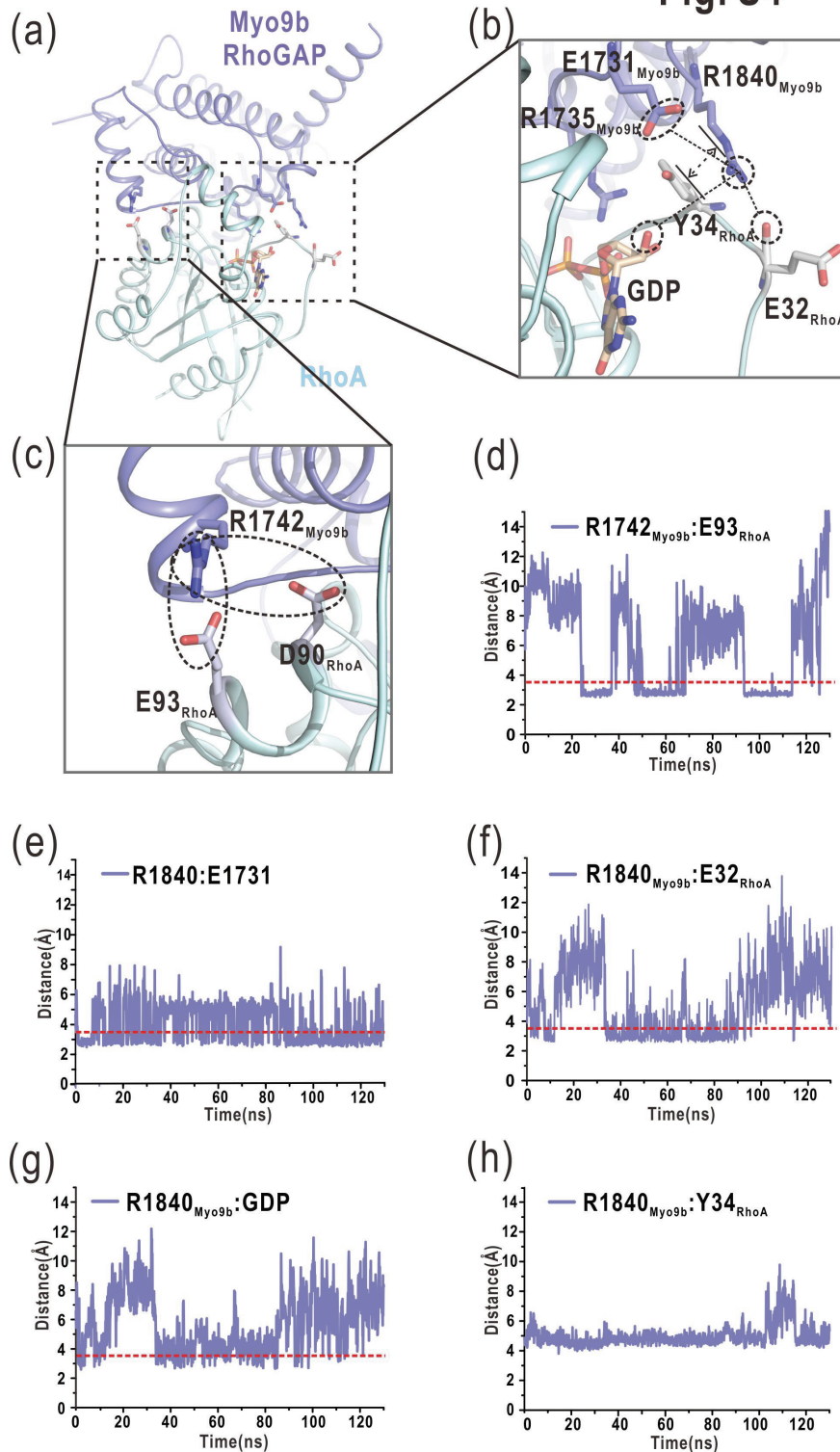


Fig. S4. The MD simulations of the Myo9b-RhoGAP/RhoA complex. (a) A ribbon diagram of a representative structure of the Myo9b-RhoGAP/RhoA complex. Myo9b-RhoGAP and RhoA are colored in blue and cyan, respectively. The selected interaction regions for R1742 and R1840 of Myo9b-RhoGAP are highlighted with dashed boxes. (b) A combined ribbon-and-stick model illustrates the interaction region for R1840. The residues and GDP that make contacts with R1840 are shown as sticks. The distances between the side-chain of R1840 and the side-chain or main-chain of other residues or GDP

are highlighted with dashed circles and lines. The distance between the side-chain of R1840 and the aromatic ring of Y34 is marked with a dashed arrow. (c) A combined ribbon and stick model illustrates the interaction region for R1742. R1742, D90 and E93 are shown as sticks and the contacts between the side-chains of them are highlighted with a dashed circle. (d) Time course of the average distance between the side-chains of R1742 and E93. The side-chain of R1742 tends to favor contacting the side-chain of E93 during the MD simulations. (e-h) Time course of the average distances between the side-chain of R1840 and the side-chain of E1731 (e), the main-chain of E32 (f), the sugar ring of GDP (g), and the aromatic ring of Y34 (h). The side-chain of R1840 intimately contacts the side-chain of E1731, the main-chain of E32, the sugar ring of GDP and the aromatic ring of Y34, and these contacts are relatively stable with certain fluctuations during the MD simulations. The hydrogen bond could be formed between the two atoms when the distance is less than 3.5 Å (highlighted by a red dashed line in each panel).

Fig. S5

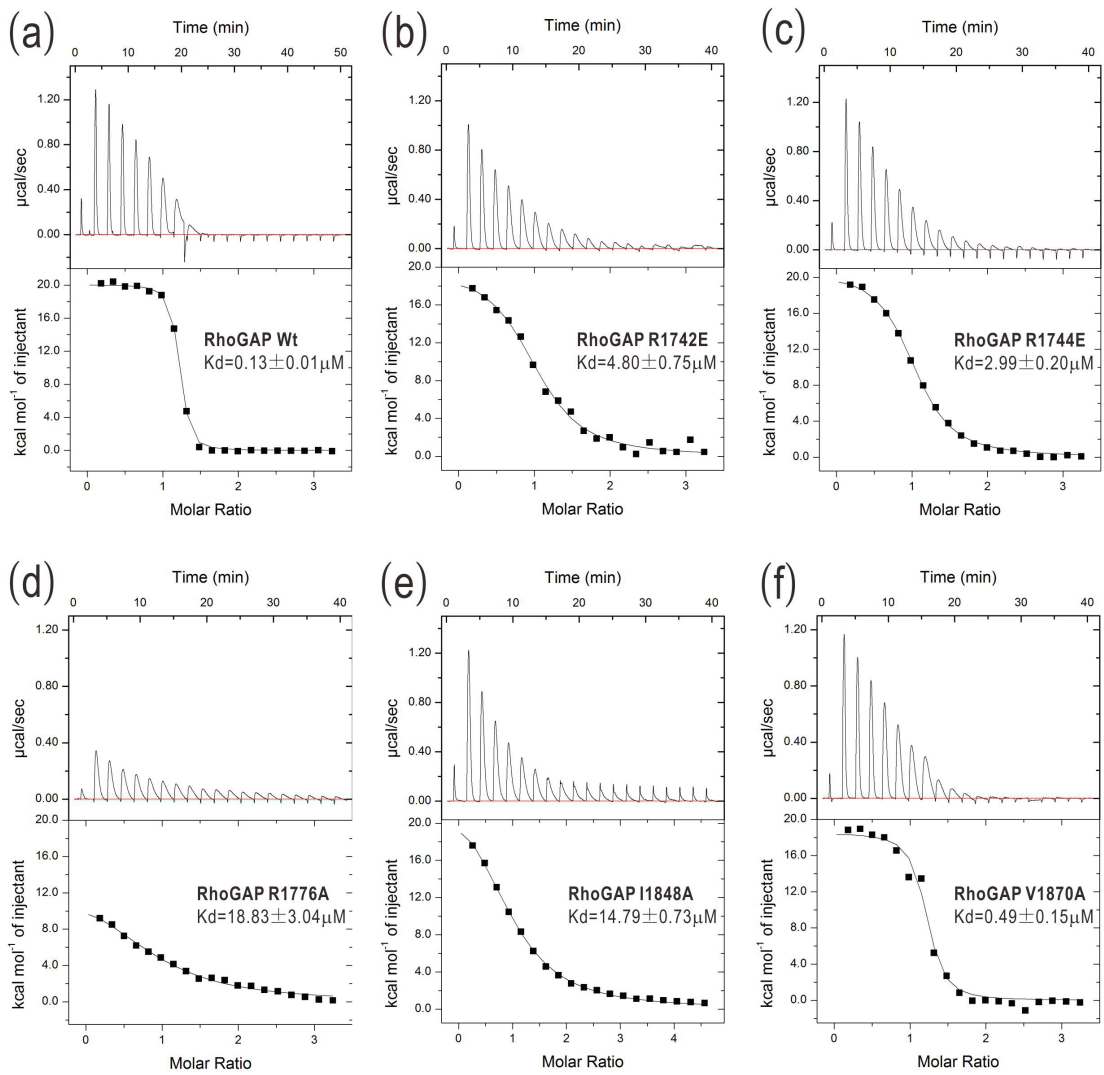


Fig. S5. The ITC assay of the binding affinities between various Myo9b-RhoGAP proteins (a-f) and RhoA. The binding affinity of each Myo9b-RhoGAP protein for RhoA is indicated in each panel. All the results were summarized in Fig. 2f.

Fig. S6

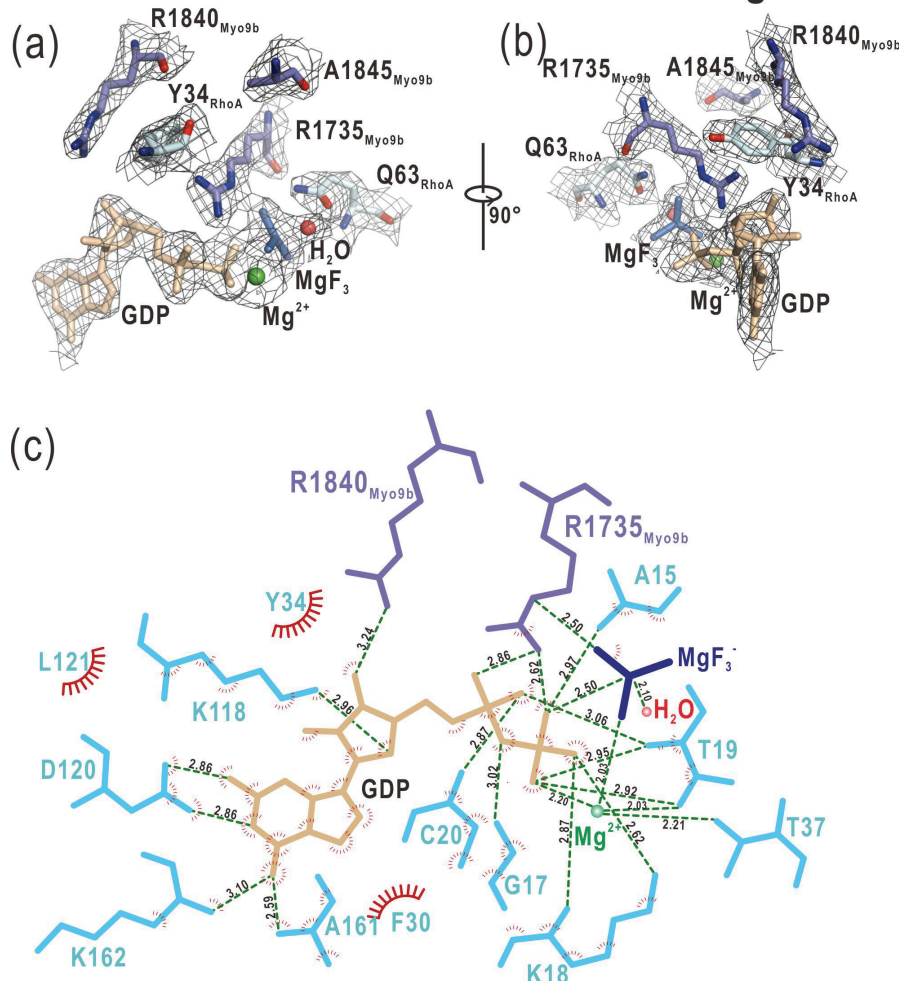


Fig. S6. The interaction network around the nucleotide in the complex structure. (a-b) A close-up view of the nucleotide and a number of surrounding essential residues in the complex structure by a stick model representation. The electron density map ($2Fo-Fc$ map) of GDP, MgF_3^- , Mg^{2+} , a putative nucleophilic water and the surrounding essential residues is shown and contoured at 1.5σ level. (c) An interaction network surrounding the nucleotide generated by LigPlus (<http://www.ebi.ac.uk/thornton-srv/software/LigPlus/>). In this drawing, GDP, MgF_3^- and the surrounding residues are shown as sticks, and Mg^{2+} and the water molecule are shown as a green and red sphere, respectively. The residues from Myo9b-RhoGAP and RhoA are colored in purple and light blue, respectively. The hydrogen bonds and salt bridges are indicated by green dashed lines and the distances between different atoms are also marked. The hydrophobic residues from RhoA for binding to the nucleotide are marked by red semi-circles with spokes indicating the directions of their side-chains.

Fig. S7

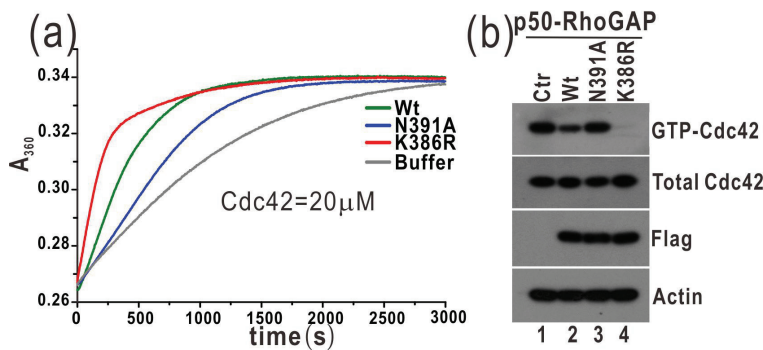


Fig. S7. Biochemical characterization of the catalytic activity of p50-RhoGAP and its mutants. (a) Time courses of GTP hydrolysis for Cdc42 (20 μ M) catalyzed by p50-RhoGAP and its mutants (40 nM). (b) Biochemical pull-down analysis of active GTP-bound Cdc42 with p50-RhoGAP and its mutants. The active Cdc42 levels were measured by GST pull-down with GST-PBD and analyzed by western blotting using the specific anti-Cdc42 antibody. The levels of total Cdc42, Flag-tagged p50-RhoGAP and the actin (as an internal loading control) in the cell lysate were also shown. Consistently, the N391A mutation impaired the catalytic activity of p50-RhoGAP, whereas the K386R mutation increased that of p50-RhoGAP. In these experiments, Cdc42 was used as a substrate for p50-RhoGAP, since p50-RhoGAP has shown the high specific activity toward Cdc42.

Fig. S8

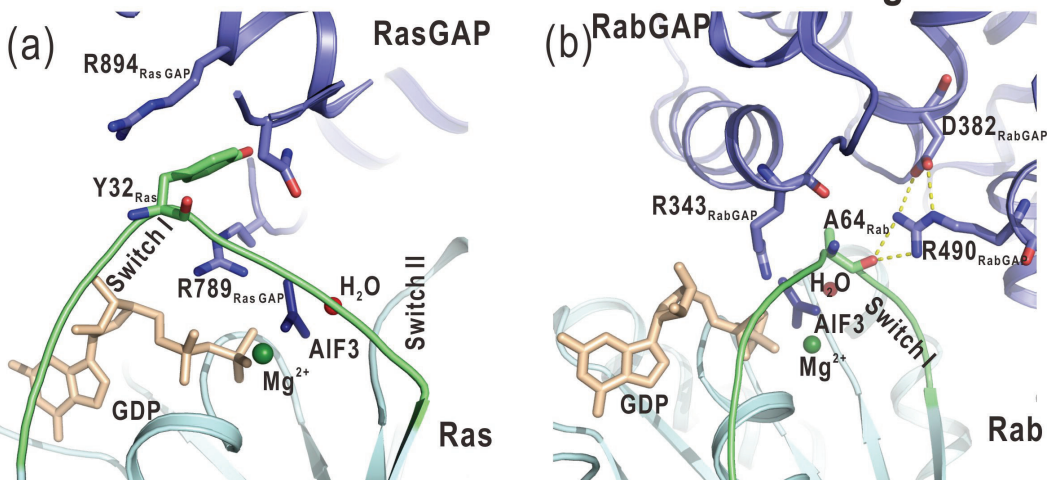


Fig. S8. The potential second arginine finger hidden in other GAP domains. (a) A combined ribbon-and-stick model illustrates the catalytic site in the structure of the RasGAP/Ras complex (PDB code: 1WQ1). The residues essential for catalysis are shown as sticks. An arginine (R894) from the RasGAP domain is also close to the Switch I loop of Ras and aligns well with the aromatic ring of Y32 from Ras. (b) A combined ribbon-and-stick model illustrates the catalytic site in the structure of the RabGAP TBC/Rab complex (PDB code: 2G77). The residues essential for catalysis are shown as sticks. Besides the catalytic arginine finger (R343), another arginine (R490) from the TBC domain forms the hydrogen-bonding interactions with the backbone of the Switch I loop of Rab and also interacts with D382 from the neighboring helix, which resembles the second arginine finger in Myo9b-RhoGAP.

Table S1: Data Collection and Refinement Statistics

<i>A. Diffraction data</i>	Myo9b-RhoGAP/RhoA complex
Wavelength (Å)	0.9791
Space group	P2 ₁ 2 ₁ 2
Unit cell parameters(Å)	a=114.1, b=90.8, c=93.6
Resolution(Å)	50.0-2.40 (2.53–2.40) ^a
No. of unique reflections	38652(5572)
Redundancy	7.0(7.2)
Mean I/σ(I)	12.8(3.0)
Completeness (%)	99.9(100.0)
R _{merge} ^b (%)	8.5(66.5)
<i>B. Structure refinement</i>	
Resolution (Å)	48.7-2.40 (2.46-2.40)
R _{work} ^c /R _{free} ^d (%)	20.3(28.3)/24.5(33.5)
R.m.s. deviation ^e	
Bonds (Å)	0.013
Angles (°)	1.29
Average B factor (Å ²)	66.0
No. of atoms	5988
Protein atoms	5772
Ligand	67
Water molecules	149
Ramachandran plot (%)	
Favored region	96.0
Allowed region	4.0
Disallowed region	0.0

^aValues in parentheses refer to the highest resolution shell.

^bR_{merge}= $\sum_h \sum_i |I_i(h) - \langle I(h) \rangle| / \sum_h \sum_i I_i(h)$, where I is the observed intensity and $\langle I \rangle$ is the average intensity of multiple observations of symmetry-related reflection h .

^cR_{work} is the R_{factor} for the working dataset. R_{factor}= $\sum ||Fo| - |Fc|| / \sum |Fo|$ where |Fo| and |Fc| are observed and calculated structure factor amplitudes respectively.

^dR_{free} is the cross-validation R_{factor} computed for a randomly chosen subset of 5% of the total number of reflections, which were not used during refinement.

^eRoot mean square deviation from ideal values.